# <u>Radiative Heat Transfer Modeling of a windowless Low-Pressure Cavity Reactor</u>

Abhishek Kumar Singh

Report Prepared for

**Austrian Marshall Plan foundation**

(13 December 2012)

TABLE OF CONTENT

LIST OF FIGURES

Page

## ABSTRACT

The presented work has been completed during my stay at the Vorarlberg University of Applied Sciences from 16 August 2012 until 19 November 2012. I gratefully acknowledge the financial support for this work by the Austrian Marshall Plan foundation.

A FORTRAN based model for the radiative transfer inside the cavity reactor has been developed. The cavity reactor consists of a closed horizontal cylinder (cavity) with an opening (aperture) and a number of horizontal tubular absorbers at the circumference of the cavity. An in-house collision-based Monte Carlo is used to optimize the aperture diameter. Two separate models are used to trace the rays from the solar simulator until they are either absorbed inside the cavity or leave the cavity through the aperture. Vegas is used to trace the rays originating from the solar simulator to the aperture of the cavity reactor. An independent collision based Monte Carlo ray tracing (MCRT) model has been developed to trace the rays from the aperture of the cavity reactor until they either get absorbed inside the cavity or leave the cavity through the aperture. Significant re-emission occurs at higher temperatures. Re-emission from the cavity surface and the absorber surface is also accounted for. A lattice Boltzmann conduction code developed at University of Florida is used for the conduction modeling in the absorbers. A zero-order Arrhenius-type chemical rate law is used to accounts for the heat consumption due to endothermic reaction inside the absorber. The finite difference (FD) method is used to model the 3-D conduction at the cavity surface. The MCRT model, FD code and the lattice Boltzmann model are coupled together to obtain the steady state temperature profile and the heat flux distribution in the absorbers and

at the surface of the cavity. The study state temperature and heat flux distribution is obtained for multiple energy input level.

A participating medium Monte Carlo ray tracing (MCRT) method is employed to trace the rays inside the porous medium of the reactor. Emission from the reacting gas inside the reactor is negligible due to the short length-scales of the porous structure. Anisotropic scattering is taken in account for the radiation modeling. Due to comparatively large particle size (around 100 micrometer) of the porous medium, geometric optics is used to determine the extinction coefficient of the participating medium. MCRT is more accurate as compared to other radiation models but it is also computationally more expensive. Due to the large optical thickness of the medium a simpler radiation model, the diffusion approximation is then used. The diffusion approximation provides strongly temperature dependent radiative conductivity, reducing the radiation problem to a steady state diffusion problem. The diffusion approximation is not accurate near the boundaries. So the more accurate $P_1$- approximation is used. It further reduces the computational time as compared to that of MCRT at the same time, increases the accuracy compared to that of diffusion approximation. The $P_1$-approximation is a first order accurate spherical harmonic method. Each of these models is used individually with the finite volume conduction model. A comparison of these three models is carried out.

## Nomenclature

$A$ = surface area of the enclosure (m$^2$)
$E_a$ = Activation energy should be experimentally determined $\left(\text{kJmol}^{-1}\right)$
$\mathrm{d}F_{\mathrm{d}A^{'}\rightarrow \mathrm{d}A}$ = generlized radiation exchange factor between
surface elements $dA^{'}$ and $dA$
$\bar{h}$ = Specific enthalpy of the reactants or products (kJ kg$^{-1}$)
$h$ = Heat transfer cofficient (Wm$^{-2}$K$^{-1}$)
$\mathrm{I}_{\nu}$ = Modified Bessel function of the first kind
$\mathrm{J}_o, \mathrm{J}_1$ = Bessel function of the first kind and
order 0 and 1 respectively.
$\mathrm{K}_{\nu}$ = Modified Bessel function of the second kind
$k$ = Thermal conductivity of the material (Wm$^{-1}$K$^{-1}$)
$k_0$ = Pre-exponential factor $\left(\text{kg m}^{-2}\text{s}^{-1}\right)$
$T(\vec{r})$ = surface temperature at location $\vec{r}$ (K)
$q(\vec{r})$ = local surface heat flux at location $\vec{r}$ (Wm$^{-2}$)
r = Radius of the back plate (m)
$r'''_{\mathrm{Fe_3O_4}}$ = Volumetric reaction rate (kg m$^3$s$^{-1}$)
$L$ = Thickness of the back plate (m)
$L_{cyl}$ = length of the cylindrical part (m)
$\varepsilon(\vec{r})$ = total hemispherical emittance of the surface at $\vec{r}$
$I_{\lambda}$ = radiative energy flux per unit solid
angle and wavelength
$\kappa_{\lambda}$ = absorption coefficient
$I_{b\lambda}$ = black body intensity
$\beta_{\lambda}$ = extinction coefficient
$\Phi$ = phase function
$\sigma_{s\lambda}$ = scattering coefficient
$G(\tau)$ = incidence radiation
$\omega_{\eta}$ = single scattering albedo
$A_1$ = Asymmetry factor
$\tau$ = optical thickness
$V_{void}$ = Volume of void space
$V_{particle}$ = Volume of particles

## Introduction

Solar thermochemical fuel production using metal/metal oxide cycle is a two-step process. The first step consists of the oxidation of a metal, typically using water to produce hydrogen and the second step consists of the thermal reduction of the metal oxide. This second step is highly endothermic, requiring significant energy input at high temperatures [1]. Concentrated solar energy is used as the energy source for thermal reduction [2, 3]. Denoting M as the used metal and MO the corresponding metal oxide, the reduction and oxidation steps cab be represented by

Reduction Step $$MO_{oxidized} \rightarrow MO_{reduced} + O_2 \,, \tag{1.1}$$

Oxidation Step $$MO_{reduced} + H_2O \rightarrow MO_{oxidized} + H_2 \,, \tag{1.2}$$

The corresponding reaction equations for $Fe_3O_4$/FeO are given by [4]

Reduction step

$$Fe_3O_4 \rightarrow 3FeO + (1/2)O_2 \,, \quad \Delta H^o_{298K} = 319.5 \text{ kJ mol}^{-1} \tag{1.3}$$

Oxidation step

$$3FeO + H_2O \rightarrow Fe_3O_4 + H_2 \,, \quad \Delta H^o_{298K} = -33.6 \text{ kJ mol}^{-1} \tag{1.4}$$

By reducing operating pressure of the reduction process, reduction temperature lowered due to LeChatelier's principle [4]. For the $Fe_3O_4$/FeO redox pair at $10^{-4}$ bar operating pressure, thermal reduction temperature falls below to 1500 $^oC$ [5]. Steinfeld et al. [6, 7, 8] used horizontal cavity reactor with a quartz window for solar thermochemical fuel production. They directly irradiated the reactant particles leading to an efficient energy transfer. The aperture window must be kept clean and cool using constant gas-flows. Also scaling up refractory windows is extremely challenging, making windowed reactors undesirable for commercial processes.

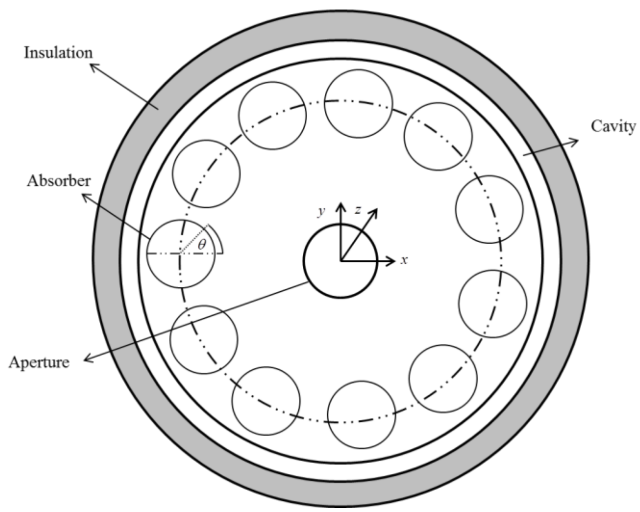


**Fig. 1.1 Schematic layout (front view) of the windowless horizontal cavity reactor.**

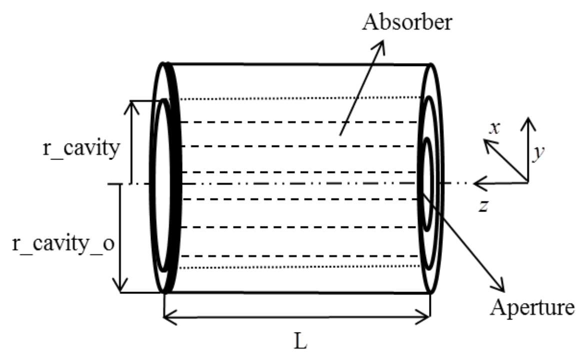


**Fig. 1.2 Schematic layout (side view) of the windowless horizontal cavity reactor.**

In the present work, a windowless horizontal cavity reactor (Fig. 1.1) is considered. The windowless horizontal cavity reactor consists of an insulated horizontal cylinder (cavity) with a small opening (aperture) and a number of tubular cylinders (absorbers) at the circumference of the cavity. The cavity allows multiple reflections of the rays so that the behavior of the cavity closely resembles that of a black body. Due to multiple reflections inside the cavity, the apparent absorptance of the cavity increases as compared to the actual absorptance of the cavity material [9, 10]. The reactants inside the absorber are indirectly heated by the solar radiations. Low pressure inside the absorbers is created using a vacuum pump.

Melchior et.al [11] performed a Monte Carlo ray tracing analysis of a vertical cavity reactor for diffusely/specularly reflecting walls, containing single tube and multiple tubes, and a selective window and a windowless aperture. In the vertical cavity reactor, a large fraction of radiations hit the cavity walls leading to low efficiency of the reactor. In the current design, absorbers cover the periphery of the cavity to facilitate maximum radiations hitting the absorbers rather than hitting the cavity. In their work, Melchior et.al did not stimulate the heat transfer inside the absorbers. Rather, they considered the net power absorbed by the reactor as a parameter and calculated the energy transfer efficiency based on the variation of this parameter. In contrast, the current analysis involves the development of a coupled model in which radiation model is integrated with the lattice Boltzmann model, accounting for the conduction inside the absorbers and the reaction rate of the reduction process.

In lab-scale experiments, the University of Florida high flux solar simulator will be used as the radiation source. Radiative transfer from the simulator to the reactor is modeled using the Vegas Monte Carlo ray tracing code. Then, the aperture diameter is optimized using the Vegas [12] code. A collision based Monte Carlo ray tracing (MCRT) model is used to further trace the rays from the aperture of the cavity until either they are absorbed inside the cavity or escape the cavity through the aperture. Re-emission from the cavity surface and absorbers surfaces is also considered. The radiation model is coupled with the lattice Boltzmann model (LBM) to obtain the temperature profile at the absorber surface. The LBM accounts for the conduction inside the porous medium of the absorber. A zero-order Arrhenius-type rate law is considered to account for the heat sink term due to the chemical reaction inside the absorber. The finite difference method is used to solve the unsteady state 3-D conduction at the cavity surface. Losses due to re-emission and convection from the cavity surface are also considered while solving for the temperature profile at the cavity surface. The radiation model, the cavity conduction code and the LBM are coupled to obtain the steady state temperature profile and the heat flux at the absorber and the cavity surface. Temperature and heat flux profile at the surface of the absorber is obtained for multiple energy input. The maximum temperature achieved at the absorber surface is 2557 K for a 5 KW energy input. This temperature is sufficient to carry out the magnetite thermal reduction process.

### 1.1 Radiation model

The schematic layout of a windowless horizontal cavity reactor with absorbers at the inner periphery is shown in Fig. 1.1 and Fig. 1.2. Ideally, the absorbers should be touching each other so that incoming rays will not hit the cavity walls. However, some clearance must be left between the absorbers due to manufacturing limitations. The Vegas code is used for optimizing the aperture diameter. The fraction of the incident radiations at the aperture from the solar simulator varying with the diameter of the aperture is shown in Figure 3. As the size of the aperture increases, the fraction of incident radiation admitted into the cavity increases; however with increased aperture size, the radiation losses through the aperture also increase. Due to a part of radiations absorbed at the solar simulator mirror surfaces, incident power at the aperture never converges to 1. Approximately 75% of the solar simulator output radiative power is incident at a 5 cm diameter aperture. For a 10 KW reactor, 5 cm diameter aperture provides the required incident heat flux at the aperture from a solar simulator of 13.3 KW output power. Rays from solar simulator are traced up to the aperture using Vegas. The MCRT code is used for further tracing the rays until they either get absorbed inside the cavity or escape through the aperture.

For a non-participating medium and assuming a refractive index of unity, the radiative heat flux leaving or going into a surface, using MCRT, is governed by the following equation.

$$q(\vec{\mathrm{r}}) = \varepsilon(\vec{\mathrm{r}})\sigma T^4(\vec{\mathrm{r}}) - \int_A \varepsilon(\vec{\mathrm{r}}^{'})\sigma T^4(\vec{\mathrm{r}}^{'}) \frac{\mathrm{d}F_{\mathrm{d}A^{'}\rightarrow \mathrm{d}A}}{\mathrm{d}A}\mathrm{d}A^{'} \tag{1.5}$$

The first term on the right hand side of eq. (1) represents the emission from the cavity/absorber surface at location $\vec{\mathrm{r}}$ and the corresponding temperature $T(\vec{\mathrm{r}})$. The second term represents the fraction of energy originally emitted from the surface at $\vec{\mathrm{r}}^{'}$, which eventually absorbed at location $\vec{\mathrm{r}}$.

Each ray is assumed to carry same amount of power. The power $Q_{\mathrm{ray}}$ carried by each ray from the simulator is given by

$$Q_{\mathrm{ray}} = \frac{Q_{\mathrm{input,simulator}}}{N_{\mathrm{ray,total}}} \tag{1.6}$$

The cavity and the absorber surfaces are assumed to be diffusely reflecting / emitting. The cavity surface and the absorber surfaces are divided in small elements of equal area.

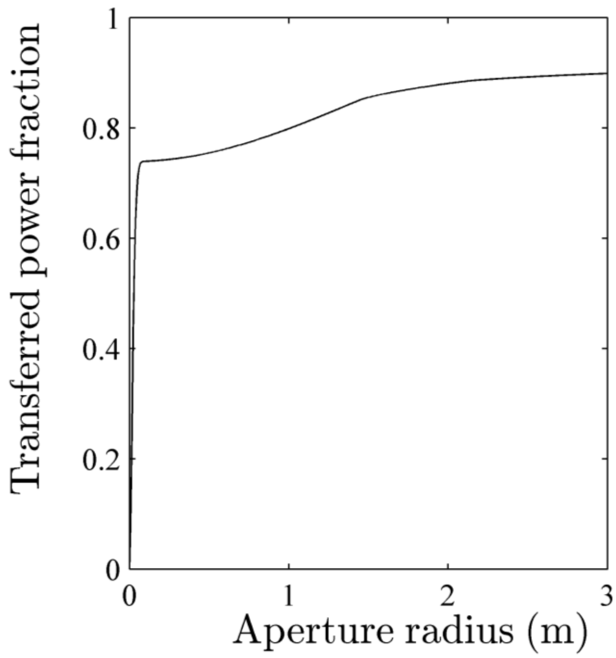


**Fig. 1.3 Variation of fraction of transferred power from the solar simulator to the aperture with increase in the aperture radius.**

The number of rays re-emitted by absorbers and the cavity surface are given by

$$N_{\mathrm{i,cavity}} = \frac{\varepsilon\sigma T^4{}_{\mathrm{i,cavity}}\mathrm{d}A_{\mathrm{i}}}{Q_{\mathrm{cavity}}} N_{\mathrm{ray,total}} \tag{1.7}$$

$$N_{\mathrm{i,absorber}} = \frac{\varepsilon\sigma T^4{}_{\mathrm{i,absorber}}\mathrm{d}A_{\mathrm{i}}}{Q_{\mathrm{absorber}}} N_{\mathrm{ray,total}} \tag{1.8}$$

Where

$$Q_{\mathrm{cavity}} = \sum_{i=1}^{n} \varepsilon\sigma T^4{}_{\mathrm{i,cavity}}\Delta A_{\mathrm{i}} \tag{1.9}$$

and $$Q_{\text{absorber}} = \sum_{i=1}^{n} \varepsilon\sigma T^{4}_{\text{i,absorber}} \Delta A_{\text{i}} \tag{1.10}$$

The lattice Boltzmann method (LBM) [14] is used for the calculation of the heat transfer inside the absorbers. The absorber heat flux calculated using MCRT is provided to the LBM to obtain temperature profile of the absorber. Due to multiple number of absorbers used in the simulation, an average heat flux approach is used to reduce the computational time of simulation. A FORTRAN based finite difference code is developed to solve the 3-D conduction within the cavity surface. The temperature profile for the cavity surface is obtained by using cavity conduction code.

## 1.2 Chemical reaction rate

The reduction of iron oxide is an endothermic reaction. The heat of the reaction is given by

$$q'''_{\text{chem}} = r'''_{\text{Fe}_3\text{O}_4}(3\bar{h}_{\text{FeO}} + 0.5\bar{h}_{\text{O}_2} - \bar{h}_{\text{Fe}_3\text{O}_4}) \tag{1.11}$$

A zero-order Arrhenius-type rate law [15, 16] is used to model the reaction rate.

$$r'''_{\text{Fe}_3\text{O}_4} = \frac{Ak_0}{\rho}\exp\left(\frac{-E_a}{RT}\right) \tag{1.12}$$

## 1.3 Cavity Conduction

The horizontal cavity reactor is divided into three parts front plate, back plate, and the horizontal cylindrical (as shown in fig. 1.4). The finite difference approach is used to solve the unsteady state conduction equation for the different parts of the cavity. Due to the geometrical complexity of the front plate, 1-D unsteady state heat conduction is assumed. For the back plate and the horizontal cylinder part, 3-D unsteady state heat conduction is solved. The Cylindrical part of the cavity interact with the front plate and back plate. Coupling of the three parts is done assuming perfect surface contact between each part.

The governing equation for a 3-D unsteady state conduction in cylindrical coordinates for no heat source term [17] is given by

$$\frac{1}{r}\frac{\partial}{\partial r}\left(rk\frac{\partial T}{\partial r}\right)+\frac{1}{r^2}\frac{\partial}{\partial \varphi}\left(k\frac{\partial T}{\partial \varphi}\right)+\frac{\partial}{\partial z}\left(k\frac{\partial T}{\partial z}\right)=\rho c\frac{\partial T}{\partial t}$$

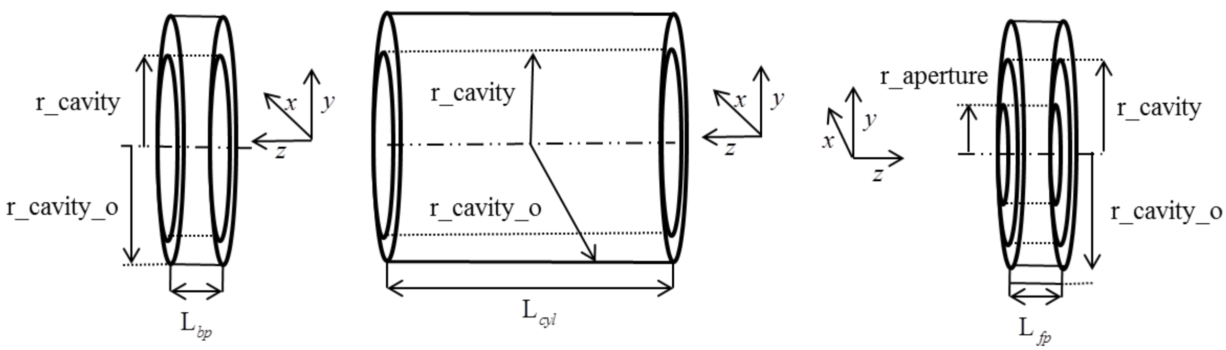


**Fig. 1.4 exploded view of the windowless horizontal cavity reactor**

*Boundary conditions*

***Cylindrical part***

BC)$_1$ @ r = $r_{cavity}$ $$-k\frac{\partial T}{\partial r}=-q''+\varepsilon\sigma T^4(\mathrm{r})$$

BC)$_2$ @ r = $r_{cavity\_o}$ $$-k\frac{\partial T}{\partial r}=h(T(\mathrm{r})-T_{ambient})+\varepsilon\sigma T^4(\mathrm{r})$$

BC)$_3$ $2\pi$ periodicity boundary condition in the $\varphi$ direction

$$T(\varphi) = T(\varphi + 2\pi) \text{ and}$$
$$\left.\frac{\partial T}{\partial \varphi}\right|_{\varphi} = \left.\frac{\partial T}{\partial \varphi}\right|_{\varphi+2\pi}$$

In the z-direction cylindrical part interacts with the front plate and back plate.

***Coupling conditions (cylindrical part with front plate and the back plate)***

Perfect contact between different parts of the cavity is assumed. The boundary conditions for the interaction of the front plate and the horizontal cylinder part of the cavity is given by

$BC)_{cp1}$ @ z = 0 and $r_{cavity} \le r \le r_{\mathrm{cavity\_o}}$

$$T_{cyl}(\mathrm{z}) = T_{fp}(\mathrm{z}) \text{ and } \left.\frac{\partial T}{\partial \mathrm{z}}\right|_{cyl} = \left.\frac{\partial T}{\partial \mathrm{z}}\right|_{fp}$$

Boundary condition for the coupling between back plate and horizontal cylinder part is given by

$BC)_{cp2}$ @ z = $L_{cyl}$ and $r_{cavity} \le r \le r_{\mathrm{cavity\_o}}$

$$T_{cyl}(\mathrm{z}) = T_{bp}(\mathrm{z}) \text{ and } \left.\frac{\partial T}{\partial \mathrm{z}}\right|_{cyl} = \left.\frac{\partial T}{\partial \mathrm{z}}\right|_{bp}$$

***Back plate***

$BC)_1$ @ r = 0 $\quad T \to \text{finite}$

$BC)_2$ @ r = $r_{cavity\_o}$ $\quad -k\frac{\partial T}{\partial r} = h(T(\mathrm{r}) - T_{ambient}) + \varepsilon\sigma T^4(\mathrm{r})$

BC)$_3$ @ z = 0 and $0 \le r < r_{\text{cavity}}$ $\quad -k\dfrac{\partial T}{\partial z} = -q'' + \varepsilon\sigma T^4(\text{z})$

BC)$_4$ @ z = $L_{bp}$ $\quad -k\dfrac{\partial T}{\partial z} = h(T(\text{z}) - T_{ambient}) + \varepsilon\sigma T^4(\text{z})$

BC)$_5$ $2\pi$ periodicity boundary condition in the $\varphi$ direction

$$T(\varphi) = T(\varphi + 2\pi) \text{ and}$$
$$\left.\frac{\partial T}{\partial \varphi}\right|_{\varphi} = \left.\frac{\partial T}{\partial \varphi}\right|_{\varphi+2\pi}$$

***Front plate***

Due to complexity of the front plate geometry, 1-D unsteady state conduction is assumed. The governing equation for this case is given by

$$\frac{\partial}{\partial z}\left(k\frac{\partial T(z)}{\partial z}\right) = \rho c\frac{\partial T}{\partial t}$$

BC)$_1$ @ z = 0 and $r_{\text{aperture}} \le r < r_{\text{cavity}}$ $\quad -k\dfrac{\partial T}{\partial z} = -q'' + \varepsilon\sigma T^4(\text{z})$

BC)$_2$ @ z = $L_{fp}$ $\quad \dfrac{\partial T}{\partial \text{z}} = 0$

### 1.4 Validation of the cavity conduction code

A 2-D steady state conduction problem (no $\varphi$ dependency) for the cavity cylinder is solved analytically. The analytical solution is used to compare the simulation results from the cavity conduction code.

The governing equation for 2-D steady state conduction in cylindrical coordinates for no heat source term [17] is given by

$$\frac{1}{r}\frac{\partial}{\partial r}\left(rk\frac{\partial T(\mathrm{r,z})}{\partial r}\right)+\frac{\partial}{\partial z}\left(k\frac{\partial T(\mathrm{r,z})}{\partial z}\right)=0$$

*Boundary conditions*

***Cylindrical part***

BC)$_1$ @ $r = r_{cavity}$ $\quad T(\mathrm{r})=T_{\mathrm{o}}$

BC)$_2$ @ $r = r_{cavity\_o}$ $\quad -k\frac{\partial T}{\partial r}=h(T(\mathrm{r})-T_{ambient})$

***Back plate***

BC)$_1$ @ $r = 0$ $\quad T\rightarrow$ finite or $\frac{\partial T}{\partial r}=0$

BC)$_2$ @ $r = r_{cavity\_o}$ $\quad -k\frac{\partial T}{\partial r}=h(T(\mathrm{r})-T_{ambient})$

BC)$_3$ @ $z = 0$ and $0\le r<r_{\mathrm{cavity}}$ $\quad T(\mathrm{z})=T_{\mathrm{o}}$

BC)$_4$ @ $z = L_{bp}$ $\quad -k\frac{\partial T}{\partial \mathrm{z}}=h(T(\mathrm{z})-T_{ambient})$

***Front plate***

The 1-D steady state conduction is assumed for the front plate. The governing equation for this case is given by

$$\frac{\partial}{\partial z}\left(k\,\frac{\partial T(z)}{\partial z}\right)=0$$

BC)$_1$ @ z = 0 and $r_{\text{aperture}} \le r < r_{\text{cavity}}$ $T(\mathrm{z}) = T_{\mathrm{o}}$

BC)$_2$ @ z = $L_{fp}$ $\frac{\partial T}{\partial z} = 0$

***Coupling conditions***

A perfect contact between different parts of the cavity is assumed. The boundary conditions for the interaction of the front plate and the horizontal cylinder part of the cavity is given by

BC)$_{cp1}$ @ z = 0 and $r_{cavity} \le r \le r_{\text{cavity\_o}}$

$$T_{cyl}(\mathrm{z}) = T_{fp}(\mathrm{z}) = T_{\mathrm{o}}$$

Boundary condition for the coupling between back plate and horizontal cylinder part is given by

BC)$_{cp2}$ @ z = $L_{cyl}$ and $r_{cavity} \le r \le r_{\text{cavity\_o}}$

$$T_{cyl}(\mathrm{z}) = T_{bp}(\mathrm{z}) = T_{o}$$

Analytical solutions based on the above governing equations and boundary conditions are given below

*Horizontal cylinder*

$$\frac{\theta}{\theta_o} = \sum_{i=1}^{\infty} \mathrm{c_n} \sin(\lambda_n z)(\mathrm{I}_o(\lambda_n r) - \frac{\mathrm{I}_o(\lambda_n a)}{\mathrm{K}_o(\lambda_n a)}\mathrm{K}_o(\lambda_n r))$$

Where

$$\mathrm{c_n} = \frac{((-1)^n - 1)}{\lambda_n (\frac{L_{cyl}}{2})(\frac{K}{h}\lambda_n (I_1(\lambda_n b) + \frac{I_o(\lambda_n a)}{K_o(\lambda_n a)} K_1(\lambda_n b)) + (I_o(\lambda_n b) - \frac{I_o(\lambda_n a)}{K_o(\lambda_n a)} K_o(\lambda_n b)))} \ ,$$

Eigen values are given by

$$\lambda_n = \frac{n\pi}{\mathrm{L}_{cyl}}, \ \text{n=1,2,3,4.....}$$

$\theta = T - T_o$ , $\theta_o = T_o - T_{ambient}$ , $a = r_{cavity}$ and $b = r_{cavity\_o}$

*Back plate*

$$\frac{\theta}{\theta_o} = \frac{2}{\mathrm{b}} \sum_{m=1}^{\infty} \frac{h}{(k\beta_m^2 + h^2)} (\cosh(\beta_m z) - (\frac{\sinh(\beta_m L) + (h/k\beta_m)\cosh(\beta_m L)}{\cosh(\beta_m L) + (h/k\beta_m)\sinh(\beta_m L)})\sinh(\beta_m z)) \frac{\mathrm{J}_o(\beta_m r)}{\mathrm{J}_o(\beta_m b)}$$

Where

Eigen values are given by

$$\beta_m = \frac{h}{k} \frac{\mathrm{J}_o(\beta_m b)}{\mathrm{J}_1(\beta_m b)}$$

$$\theta = T - T_o \quad , \theta_o = T_o - T_{ambient} \text{ , and } \quad b = r_{cavity\_o}$$

*Front plate*

$$T = T_o$$

In figs 1.5 and 1.6, a comparison of contour lines for the analytical solution and the modeling result for the horizontal cylindrical part and the back plate part of the cavity respectively, is shown. The modeling result shows the conformity with the analytical solution.

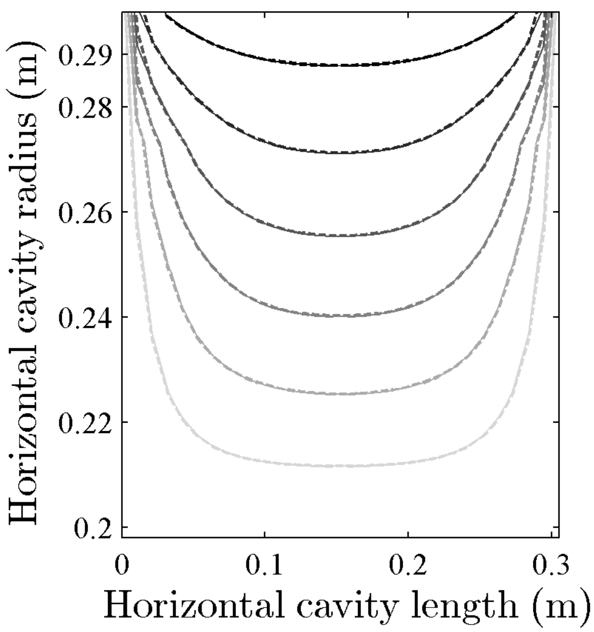


**Fig.1.5 Comparison of analytical solution (solid contour lines) and the modeling result (dotted contour lines) within the horizontal part of the cavity.**

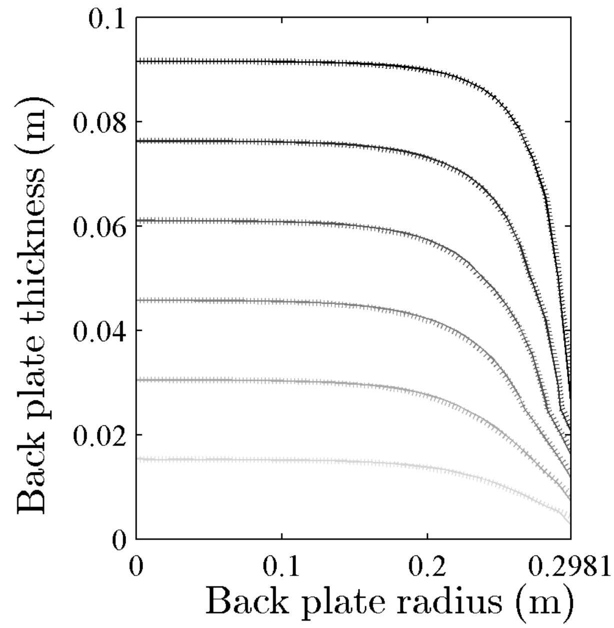


**Fig.1.6 Comparison of analytical solution (solid contour lines) and the modeling result (dotted contour lines) within the back plate part of the cavity.**

## 1.5 Process flow diagram

Figure 1.7 describe the process flow for the coupled model consisting of MCRT model, cavity conduction model and LBM.

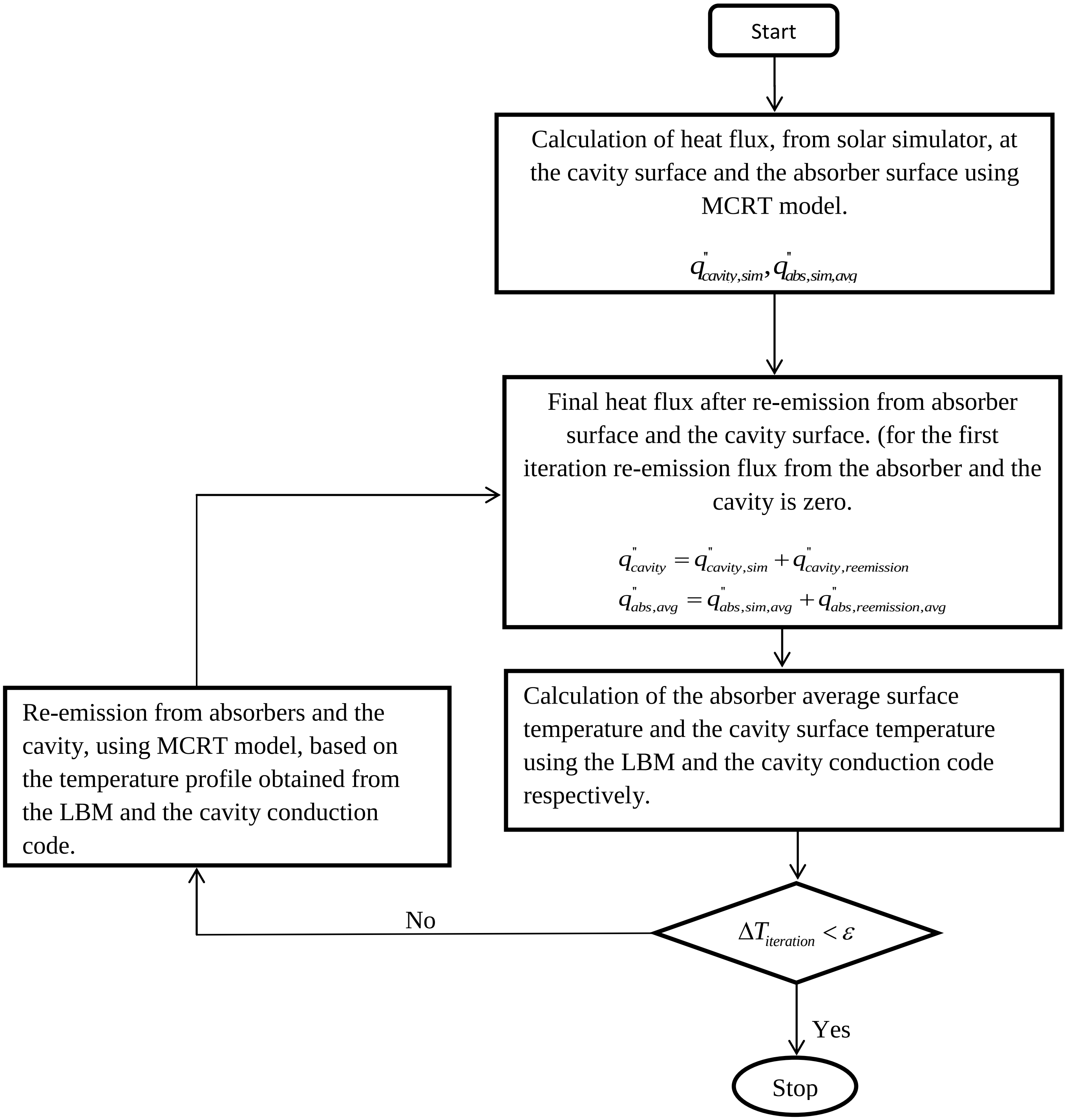


**Fig. 1.7 Process flow diagram for the cavity coupled model**

## 1.6 Results

Figure 1.8, shows the steady state average temperature distribution of the absorber inside the cavity for a 1.25 KW solar simulator power input.

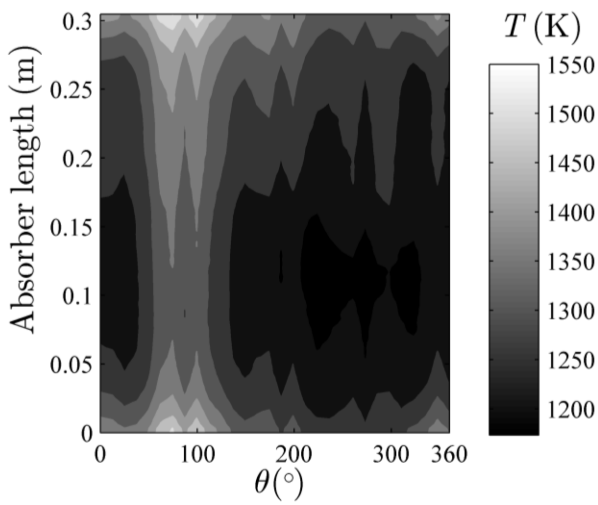


**Fig.1.8 Steady state temperature profile at the surface of the absorber (max T= 1550 K).**

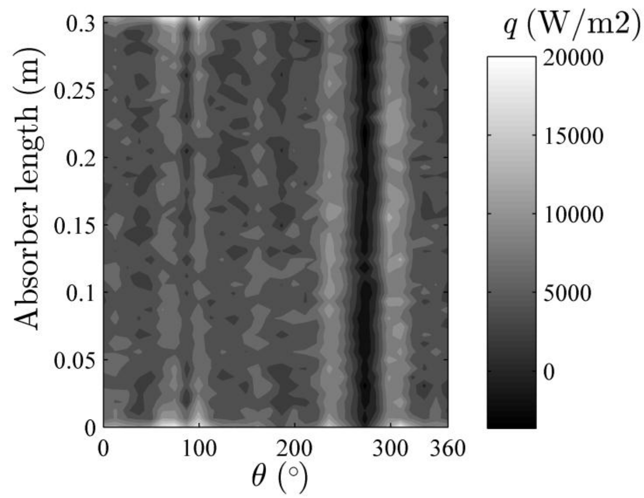


**Fig.1.9 Steady state heat flux profile at the surface of the absorber.**

The maximum steady state temperature reached in the cavity is 1550 K. There some high temperature regions at the absorber's surface. In most parts of the absorbers the surface temperature lies between 1200 and 1250 K. Fig 1.9 shows the steady state heat flux distribution at the surface of the absorber.

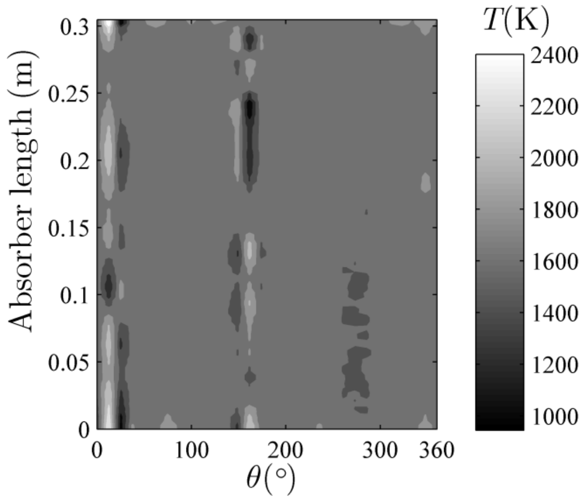


Fig. 1.10 Steady state temperature profile at the surface of the absorber (max T= 2557 K).

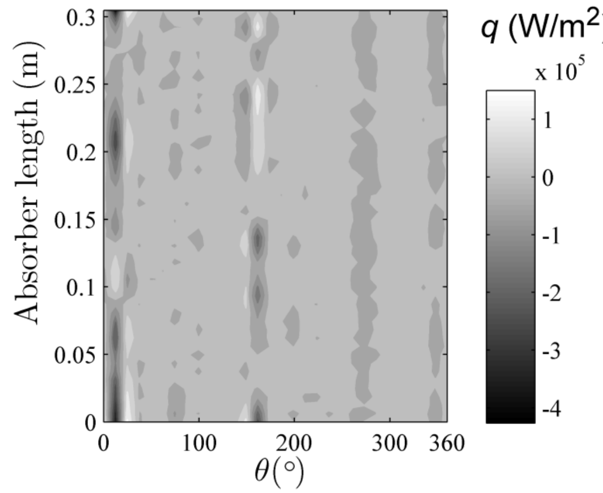


Fig.1.11 Steady state heat flux profile at the surface of the absorber.

In figure 1.10, steady state temperature distribution at the absorber surface is shown for a simulator power input of 5 kW. The maximum temperature reached is 2557 K. Absorber surface temperature increases with the increase in the power input. For the $Fe_3O_4$ reduction process (eq. 3) around 1500 $^oC$ temperature is needed at $10^{-4}$ bar pressure, which can be achieved by using high input power of the simulator. Figure 1.11 shows the steady state heat flux profile at the surface of the absorber for 5 kW power input.

**Conclusion**

A radiation model has been developed for a windowless horizontal cavity reactor. The Vegas code has been used to optimize the aperture diameter of the cavity. A cavity conduction model has also been developed for a 3-D unsteady state conduction at the cavity surface. The lattice Boltzmann model developed at University of Florida has been used for conduction modeling inside the absorbers. These models have been integrated together and used for investigating the effect of reactor length and diameter on the steady state temperature and flux distribution at the surface of the absorber. Except some regions of the absorber surface, temperature distribution is found to be uniform. The maximum temperature reached is 2557 K for a 5 kW solar power input. In future studies, the effect of different lengths and diameters of the cavity on steady state temperature distribution and flux distribution will be considered.

# RADIATION MODELING IN A PARTICIPATING MEDIUM

## Introduction

Radiation is the predominant mode of heat transfer in many high temperature engineering applications [18]. Particularly in porous materials or media containing particulates radiation heat transfer [19,20] plays an important role. Fluidized beds, packed beds, catalytic reactors, combustors, soot and fly ash, sprayed fluid, porous and reticulate ceramics, microspheres and multilayered particles are typical applications of porous media [21]. For the purpose of radiation modeling, only the porous matrix is considered as a participating medium. The reacting gases are ignored in modeling since they contribute less than 5 % to the radiation heat transfer [22]

The Monte Carlo ray tracing (MCRT) in a participating medium is used for the radiation modeling. In classical MCRT, photon bundles are traced until they are absorbed inside the system or lost to the surroundings [23]. MCRT can handle any arbitrary geometry of the system. For large numbers of photon bundles MCRT results converge towards the exact solution. MCRT can be used easily to solve non-gray, non-isothermal and anisotropic problems [23]. However, due to the statistical nature of MCRT model, a large sample of photon bundles needs to be traced, making it computationally expensive [13].

The diffusion approximation is an efficient alternative method, which can be easily applied since the porous matrix considered is an optically thick medium. It is a simpler model and computationally less expensive [13]. The radiation heat transfer inside the optically thick porous media is due to local emission and absorption of the thermal radiations [24] thereby justifying the use of diffusion approximation.

One major drawback of diffusion approximation is the inaccuracy at the system boundaries [25]. The $P_1$- approximation, a first-order spherical harmonics method, is used to counter the deficiency of the diffusion approximation. In the $P_1$-approximation, the integro-differential radiative transfer equation is converted to a set of partial differential equations [13]. These partial differential equations can be solved by employing the common numerical schemes. This method is computationally less expensive compared to the MCRT method and is more accurate at the boundaries than the diffusion approximation method.

The Radiative properties of the porous media are determined using geometrical optics for large particles [13]. An experimental specimen is used to determine the particle volume fraction of the porous medium. Linear anisotropic scattering is assumed inside the porous medium. Boundaries are assumed to be perfectly insulated and diffusely emitting/reflecting. All the above models are then individually integrated with the conduction model developed by Li *et al.* [14]. Since MCRT is the most accurate of the methods considered; a comparison of the diffusion approximation and the $P_1$-approximation with the MCRT is performed. Figure 2.1 shows the schematic layout of the porous medium considered for the study.

### 2.1 Monte Carlo Ray tracing model

A Monte Carlo ray tracing (MCRT) method for a participating medium is used for the radiation modeling in a porous medium. A participating medium emits, absorbs and

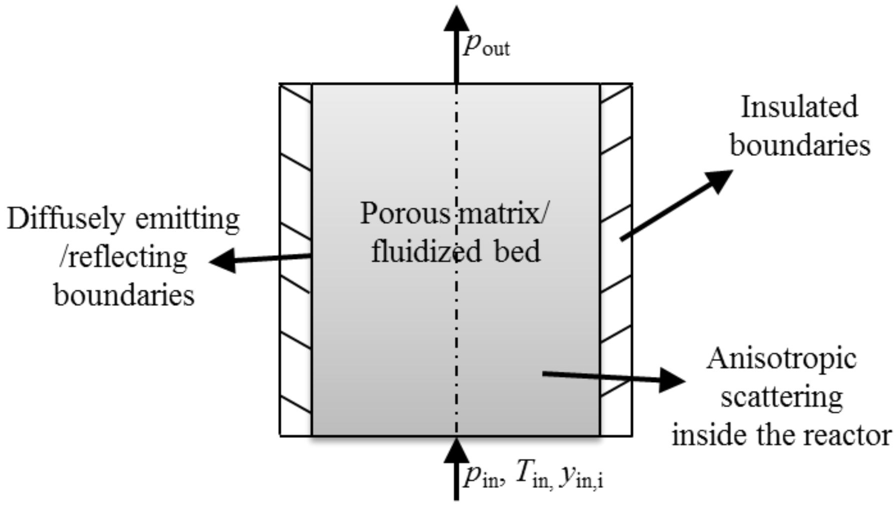


**Fig. 2.1 Schematic layout of the porous matrix inside the reactor.**

scatter radiations. The Radiative heat transfer in a participating medium is govern by the following equation (RTE) [13]

$$\frac{\mathrm{d}I_{\lambda}}{\mathrm{d}s} = \kappa_{\lambda} I_{b\lambda} - \beta_{\lambda} I_{\lambda} + \frac{\sigma_{s\lambda}}{4\pi}\int_{4\pi} I_{\lambda}(\hat{\mathrm{s}}_i)\Phi(\hat{\mathrm{s}}_i,\hat{\mathrm{s}})d\Omega_i, \qquad (2.1)$$

The first term on the RHS of above equation expresses the augmentation of intensity by emission. The second term expresses the reduction of intensity by extinction. The last term quantifies augmentation by in-scattering, where the phase function $\Phi(\hat{\mathrm{s}}_i,\hat{\mathrm{s}})$ is the probability that a ray is scattered from direction $\hat{\mathrm{s}}_i$ into direction $\hat{\mathrm{s}}$. The porous medium (fig. 2.1) is discretized into smaller sub-volumes. Each sub-volume is supposed to have constant radiative properties. The divergence of heat flux is given by [23]

$$\nabla.\mathrm{q}_r = \int_0^{\infty} \kappa_{\lambda}(4\pi I_{\lambda b} - \int_{4\pi} I_{\lambda}\mathrm{d}\Omega)\mathrm{d}\lambda \qquad (2.2)$$

The porous matrix is assumed to be nongray, absorbing, emitting and linear anisotropically scattering participating medium. The medium particles are assumed to be opaque and spherical in shape - a reasonable assumption for irregularly shaped and randomly oriented particles [19].

#### 2.1.1 Random number relations

The point of emission from the surface of a sub-volume is given by

In the r-direction $r = r_i + \Re dr$ (2.3)

In the z-direction $z = z_i + \Re dz$ (2.4)

Where $\Re$ is the random number between 0 and 1.

The emission direction of the ray from the emission point is given by

Azimuthal angle $\psi = 2\pi\ \Re_\psi$ (2.5)

And polar angle $\theta = \cos^{-1}(1 - 2\Re_\theta)$ (2.6)

By using the above random number relations for azimuthal angle and polar angle, the direction cosines can be used to obtain the direction of the emitted ray. The photon bundle emitted is traced until it is absorbed inside the medium or leaves the boundary. The emitted photon bundle is not absorbed and allowed to move further until the below criterion is satisfied.

$$\int_0^s \kappa_\lambda ds \ < \ \int_0^{l_\kappa} \kappa_\lambda ds \ = \ \mathrm{In}(\frac{1}{\Re_\kappa}) \qquad (2.7)$$

Where $\int_0^s \kappa_\lambda ds \cong \sum_k \kappa_{\lambda_k} s_k$ (for k sub-volumes of constant absorption coefficient). The photon path length ($l_k$) is given by $l_k = \frac{1}{\kappa_\lambda} \text{In}(\frac{1}{\Re_\kappa})$ .

Similarly for the scattering, the distance a ray travels before getting scattered is given by

$$\int_0^s \sigma_{s,\lambda} ds < \int_0^{l_\sigma} \sigma_{s,\lambda} ds = \text{In}(\frac{1}{\Re_\sigma}) \tag{2.8}$$

Where $l_\sigma = \frac{1}{\sigma_{s\lambda}} \text{In}(\frac{1}{\Re_\sigma})$

The azimuthal angle and polar angle of the scattered ray for linear anisotropic scattering is given by

Azimuthal angle $$\psi_r = 2\pi \ \Re_{\psi_r} \tag{2.9}$$

Polar angle $$\Re_\theta = \frac{1}{2}(1 - \cos\theta + \frac{A_1}{2}\sin^2\theta) \tag{2.10}$$

The new direction vector can be found by introducing a local coordinate system at the point of scattering and using above angles.

## 2.2 Diffusion Approximation

If the optical thickness of a medium is too high ( $\tau_\eta = \int_0^s \beta_\eta \mathrm{d}s >> 1$ ), the relatively simpler diffusion approximation can be used for the radiation modeling inside a porous medium [13] . The below equation can be used to obtain the heat flux

$$q = -\frac{16n^2\sigma T^3}{3\beta_R}\frac{dT}{dz} \tag{2.11}$$

A strongly temperature dependent Radiative conductivity can also be defined from the above equation as

$$k_R = \frac{16n^2\sigma T^3}{3\beta_R} \tag{2.12}$$

Where the Rosseland mean extinction coefficient ($\beta_R$) is given by

$$\frac{1}{\beta_R} = \frac{\pi}{4\sigma T^3}\int_0^\infty \frac{1}{\beta_\eta}\frac{dI_{b\eta}}{dT}d\eta \tag{2.13}$$

This reduces the radiation problem to a simple diffusion problem with strongly temperature dependent conductivity. The diffusion approximation is not accurate at the system boundaries [25].

## 2.3 $P_1$- Approximation

The Radiative transfer equation (eq. 2.1) is an integro-differential equation in six independent variables: 3 space coordinates, 2 direction coordinates and a wave length coordinate. The high dimensionality of the problem the method of spherical harmonics can be used to transform this equation into a set of partial differential equations with a higher order of accuracy. The $P_1$-approximation is the lowest order and most used spherical harmonics method. The governing equation is a Helmholtz equation:

$$\nabla_{\tau}^{2}G-(1-\omega)(3-A_1\omega)G=-(1-\omega)(3-A_1\omega)4\pi I_b \qquad (2.14)$$

The Incidence radiation is given by

$$G(\tau)=\int_{4\pi} I(\tau,\hat{s}_i)d\Omega_i \qquad (2.15)$$

The single scattering albedo is given by $\omega_\eta=\dfrac{\sigma_{s\eta}}{\beta_\eta}$ (2.16)

### 2.3.1 Boundary conditions

BC)$_1$ @ z=0 $$-\frac{(2-\varepsilon)}{\varepsilon}\frac{2}{(3-A_1\omega)}\frac{\partial G}{\partial z}+G=4\pi I_{b\omega} \qquad (2.17)$$

BC)$_2$ @ z=h $$\frac{(2-\varepsilon)}{\varepsilon}\frac{2}{(3-A_1\omega)}\frac{\partial G}{\partial z}+G=4\pi I_{b\omega} \qquad (2.18)$$

BC)$_3$ @ r=R $$\frac{(2-\varepsilon)}{\varepsilon}\frac{2}{(3-A_1\omega)}\frac{\partial G}{\partial r}+G=4\pi I_{b\omega} \qquad (2.19)$$

A FORTRAN based finite difference model is developed to solve the governing equation using the boundary conditions.

## 2.4 Radiative properties

Radiative properties of the material are calculated by using the experimental specimen of the porous media. Particle size of the medium is between 75 and 100 $\mu\text{m}$. Based on the particle size and the weight of the experimental specimen particle volume fraction ($f_V$) is calculated assuming particles are spherical in shape with uniform distribution in the experimental specimen.

$$f_v = \frac{V_{void}}{V_{particle}} \tag{2.20}$$

For the given particle size and $f_v$ geometric optics assumption is valid. Based on above assumptions, the extinction coefficient is calculated using below equations.

The DC resistivity ( $\rho_{dc}$ ) for iron is given by [26]

$$\rho_{dc} = (\mathrm{A}_1 + \mathrm{B}_1 T + \mathrm{C}_1 T^2 + \mathrm{D}_1 T^3) 10^{-6} \tag{2.21}$$

The DC conductivity is given by $\sigma_{dc} = \frac{1}{\rho_{dc}}$ (2.22)

According to the Hagen-Rubens relation [27] the index of refraction (*n*) is given by

$$n \simeq \sqrt{30 \lambda \sigma_{dc}} \tag{2.23}$$

For *n* >> 1, the spectral hemispherical reflectivity ( $\rho_{n,\lambda}$ ) can be approximated by

$$\rho_{n,\lambda} = 1 - \frac{2}{n} + \frac{2}{n^2} \tag{2.24}$$

Using eq. (2.24) and Hagen-Rubens relation the spectral hemispherical reflectivity can be determine by

$$\rho_{\lambda} = 1 - \frac{2}{\sqrt{30 \lambda \sigma_{dc}}} + \frac{2}{30 \lambda \sigma_{dc}} \tag{2.25}$$

The absorption, scattering and extinction coefficient can be calculated by using the following equations

$$\kappa_\lambda = N_p(1-\rho_\lambda)\pi a^2 \tag{2.26}$$

$$\sigma_\lambda = N_p \rho_\lambda \pi a^2 \tag{2.27}$$

$$\beta = \kappa_\lambda + \sigma_\lambda \tag{2.28}$$

## 2.5 Comparison of different radiation models

The models described above are individually integrated with the conduction model developed by Li *et al.* [14] at University of Florida and the effect of these different radiation models on the temperature profile of the porous medium is analyzed. To test the transient evolution of conduction and radiation heat transfer, the following initial condition is applied:

*T*(z=0, r)=*T*(z=H, r)=1000K;

*T*(z/H=0.5, r)=250K and the initial temperature is linear in the z-direction.

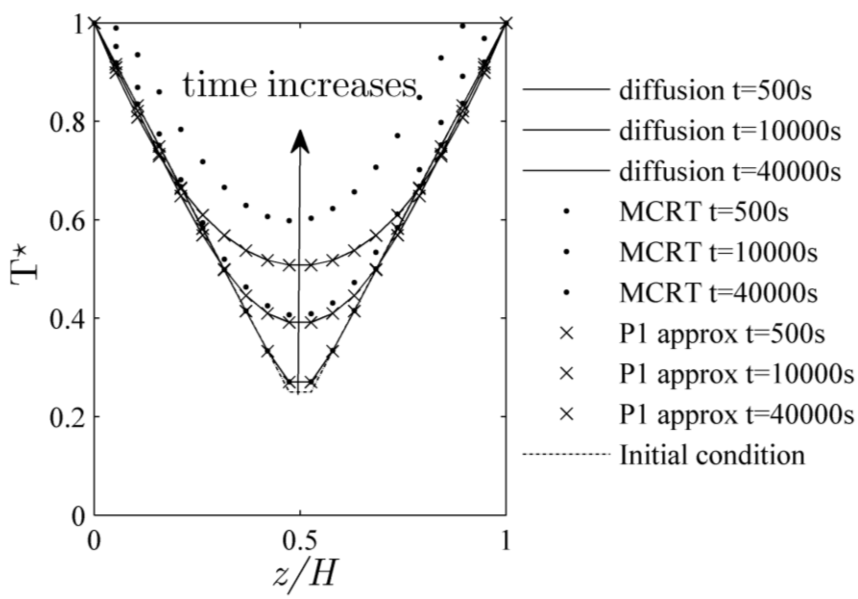


**Fig. 2.2 Effect of different radiation models on the temperature profile of the porous medium.**

Figure 2.2 shows the variation of the temperature with the increase of time based on the different radiation models employed. The MCRT model is the basis of comparison for other two models. In the beginning of the process, $P_1$-approximation and diffusion approximation shows convergence to the MCRT model. As time increases, convergence of both $P_1$-approximation and diffusion approximation decreases. The $P_1$-approximation and the diffusion approximation give similar results. So for an optically thick participating medium, both the $P_1$-approximation and the diffusion approximation can be used. Since the diffusion approximation is particularly easy to implement and computationally less expensive than the $P_1$-approximation, the use of the diffusion approximation is recommended over $P_1$-approximation in optically thick participating media. In the next chapter the diffusion approximation is integrated with the finite volume conduction model and the random walk transport of species model. The coupled model is used to investigate the effect of different input parameters on the hydrogen production.

In the future studies MCRT and $P_1$-approximation will be used individually with the coupled model and their effect on the hydrogen production will be investigated.

## References


[1] Nakamura T. Hydrogen production from water utilizing solar heat at high temperatures. Solar Energy 1976; 19: 467-475.

[2] Steinfeld, A. Energy-The International Journal, 1977, 22,311

[3] Steinfeld, A.,Kuhn,P.,Reller,A.Palumbo,R.,Murray,J., and Tamaura, Y., International Journal of Hydrogen Energy,1998,23,767.

[4] N. Gokon, S. Takahashi, H. Yamamoto, T. Kodama .Thermochemical two-step water-splitting reactor with internally circulating fluidized bed for thermal reduction of ferrite particles.

[5] Nobuyuki Gokon, Hiroko Murayama, Jun Umeda, Tsuyoshi Hatamachi,Tatsuya Kodama .Monoclinic zirconia-supported $Fe_3O_4$ for the two-step water-splitting thermochemical cycle at high thermal reduction temperatures of 1400–1600 $^{o}$C. International Journal of Hydrogen Energy, 34(2009),1208-1217.

[6] Steinfeld, A., Solar hydrogen production via a two-step water-splitting thermochemical cycle based on Zn/ZnO redox reactions. International Journal of Hydrogen energy ( 2002),611-619.

[7] Steinfeld A., Brack M. , Meier A.,Weidenkaff A., and Wuillemin D. A solar chemical reactor for co-productio of Zinc and Synthesis gas. Energy (1998) ,23, 803-814.

[8] A. Z'Graggena, P. Hauetera, D. Trommera,M. Romerob, J.C. de Jesusc, and A. Steinfeld. Hydrogen production by steam-gasification of petroleum coke using concentrated solar power-II Reactor design, testing, and modeling.

[9] Siegel, R., and Howell, J. R., 1992, Thermal Radiation Heat Transfer, 3rd ed., Hemisphere, Corporation, Washington. International Journal of Hydrogen Energy 31 (2006) 797 – 811.

[10] Steinfeld, A., 1991, Apparent Absorptance for Diffusely and Specularly Reflecting Spherical Cavities, Int. J. Heat Mass Transfer, 347, pp. 1895–1897.

[11] Mechoir, T.,and Steinfeld, A., Radiative Transfer Within a Cylindrical Cavity With Diffusely/Specularly Reflecting Inner Walls Containing an Array of Tubular Absorbers.

[12] Petrasch, J., 2002, Thermal Modeling of Solar Chemical Reactors: Transient Behavior, Radiative Transfer, MS thesis, ETH-Zürich.

[13] Modest M. Radiative heat transfer, Second edition,2003.

[14] Like Li, Renwei Mei, and James F. Klausner, Boundary conditions for thermal lattice Boltzmann equation method, Journal of Computational Physics, 2012.

[15] Müller R., Lipiński, W., and Steinfeld, A Transient heat transfer in a directly-irradiated solar chemical reactor for the thermal dissociation of ZnO. Applied Thermal Engineering, 28 (2008) 524-531.

[16] Loutzenhiser P.G., Meier A., and Steinfeld A., Review of the two-step $H_2O/CO_2$-splitting solar thermochemical cycle based on Zn/ZnO redox reactions. Materials, 3 (2010) 4922-4938.

[17] Ozisik, N. Heat Conduction, second edition (1993).

[18] Gokmen Demirkaya, Faruk Arinc, Nevin Selc-uk,, Isil Ayranci . Comparison between performances of Monte Carlo method and method of lines solution of discrete ordinates method. Journal of Quantitative Spectroscopy & Radiative Transfer, 2005 93.

[19] Peter von Zedtwitz and Aldo Steinfeld. Steam-Gasification of Coal in a Fluidized-Bed/Packed-Bed Reactor Exposed to Concentrated Thermal RadiationsModeling and Experimental Validation. Ind. Eng. Chem. Res. 2005, 44, 3852-3861.

[20] Dominique Baillis, Jean-Francois Sacadura. Thermal radiation properties of dispersed media: theoretical prediction and experimental characterization. Journal of Quantitative Spectroscopy & Radiative Transfer, 2000, 67 , 327-363.

[21] Subhash Mishra and Manohar Prasad. Radiative heat transfer in participating media- A review. Sadhana, 1998, vol.23, part2, pp. 213-232.

[22] Hirsch, D.; Steinfeld, A. Radiative Transfer in a Solar Chemical Reactor for the Co-Production of Hydrogen and Carbon by Thermal Decomposition of Methane. Chem. Eng. Sci. 2004, 59, 5771-5778.

[23] Petrasch J. Reactive flows in porous media. 2009

[24] Muller R, Lipinski W., Steinfield A. Transient heat transfer in a directly-irradiated solar chemical reactor for the thermal dissociation of ZnO. Applied Thermal Engineering, 2008, 28 , 524-531.

[25] Deissler, R.G. Diffusion approximation for thermal radiation in gases with jump boundary conditions. ASME Journal of heat transfer, 1964,vol. 86 , pp. 240-246.

[26] Touloukian, Y. S.; DeWitt, D. P. Thermophysical Properties of Matter: Thermal Radiative Properties - Nonmetallic Solids; Plenum: New York, 1972; Vol. 8.

[27] Hagen,E. and H. Rubens:Metallic reflection. Annalen der Physik, 1900, vol. 1, no. 2, pp. 352-375.

Curriculum Vitae

# Abhishek Kumar Singh

1111 SW 16th Avenue, #35, Gainesville, FL – 32601 Phone: 352-301-1788 abhishekksingh@ufl.edu

## Education

**University of Florida, Department of Mechanical and Aerospace Engineering** **Current GPA:** 3.66/4.0
**Doctor of Philosophy in Mechanical Engineering**
Thesis: Multi-scale, multi physics modeling of thermo-chemical iron/iron oxide cycle for fuel production.

## Work Experience

**J P Morgan Chase, Mumbai, India** May 2008 – July 2009
**developer, Private Banking technology**

Created a trade monitoring system through which supervisors can monitor trades done by customers. Involved in design and programming part of the project and support to the system integration testing.

**Accenture Pvt. Ltd, Mumbai, India** June 2006 – May 2008
**Software Engineer, Travelers insurance group**

The System involved maintaining a Data Warehouse system to improve overall quality and productivity of existing processes and deploying reliable and accurate information. Involved in production support and enhancement of the process according to the client requirement.

## Research

**Multiphysics model for the windowless cavity reactor**
Developed a FORTRAN based numerical radiation and conduction model for a windowless cavity reactor. A parametric study has been performed to optimize the geometry of the cavity reactor.

**Beam down optimization for Thermogravimeter**
The open source VEGAS code has been utilized to obtain maximum heat flux for the thermogravimeter using plane, elliptical and hyperbolic mirrors. An optimized configuration of mirror has been obtained for the thermogravimeter.

**Radiation modeling for continuum Multiphysics model for the looping cycle**
A FORTRAN based Monte Carlo ray tracing code for participating media was developed to simulate the Radiative heat transfer in the reactor.

**Thermal Management of the hydrogen production plant**
Plant layouts that efficiently integrate Syngas feed stream from conventional gasifier and maximize hydrogen production were developed using a MATLAB based model.

**Thermodynamic analysis of the Iron/Iron oxide looping cycle**
A MATLAB based code was developed to carry out open system equilibrium thermodynamic analysis to obtain the favorable operating conditions for oxidation/reduction processes of the looping cycle.

**Finite Volume Calculation for incompressible turbulent axisymmetric flow in a closed conduit**
Developed a FORTAN based code for turbulent flow calculations in axisymmetric geometry of a combustion chamber to obtain optimized operating conditions for the combustion chamber.

**Study and improvement in the productivity of engine assembly line.**
Productivity of TATA Motors engine assembly line was improved by incorporating low cost automation. A trolley was designed using zero gravity principal to ease the operation of lifting radiator by the operator. Through this project identification of areas where loopholes and bottleneck operations existed was carried out.

## Publications

Singh A, Al-Raqom F, Klausner J, and Petrasch J. Production of Hydrogen via an Iron/Iron Oxide Looping Cycle: Thermodynamic Modeling and Experimental Validation. International Journal of Hydrogen Energy, 36(2012) 10674-10682.

Singh A, Al-Raqom F, Klausner J, and Petrasch J. Hydrogen production via the iron/iron oxide looping cycle. Proceedings of ASME 2011 5th International Conference on Energy Sustainability, Engineering and Technology Conference ESFuelCell; 2011.